Water Adsorption on MgO Surfaces: A Vibrational Analysis

Maria Dekermenjian, Alexandre Merlen, Andreas Ruediger, Michel Rérat

crystals

MDPI

Article

Water Adsorption on MgO Surfaces: A Vibrational Analysis

Maria Dekermenjian [1], Alexandre Merlen [2,*], Andreas Ruediger [1] and Michel Rérat [3,*]

[1] EMT-INRS (Centre Énergie Matériaux Télécommunications, Institut National de la Recherche Scientifique), Varennes, QC H2X 1E3, Canada; maria.dekermenjian@inrs.ca (M.D.); andreas.ruediger@inrs.ca (A.R.)
[2] MAPIEM (Matériaux Polymères Interfaces Environnement Marin), University of Toulon, 83130 La Garde, France
[3] CNRS, Institut des Sciences Analytiques et de Physico-Chimie pour l'Environnement et les Matériaux, Energy Environmnt Solutions, Université de Pau et des Pays de l'Adour, 64000 Pau, France
* Correspondence: merlen@univ-tln.fr (A.M.); michel.rerat@univ-pau.fr (M.R.)

Abstract: Using DFT calculations, we have considered different adsorption configurations of water molecules on MgO surfaces. In some cases, we have observed a chemical reaction between water and the surface, with the formation of hydroxyl groups. We have systematically compared the calculated Raman spectra of the final optimized structures with the measured spectra from MgO nanoparticles. Our results confirm the high reactivity of MgO surfaces with water. Some obtained structures can be considered precursors for the transformation of MgO into $Mg(OH)_2$. We suggest that some of them could be identified using Raman spectroscopy. Our study confirms the high potentiality of Raman spectroscopy, associated with numerical calculations, for the study of chemical reactivity of nanoparticles.

Keywords: DFT; surfaces; Raman spectroscopy; MgO nanoparticles

Citation: Dekermenjian, M.; Merlen, A.; Ruediger, A.; Rérat, M. Water Adsorption on MgO Surfaces: A Vibrational Analysis. *Crystals* **2023**, *13*, 1153. https://doi.org/10.3390/cryst13081153

Academic Editors: Chiara Castiglioni and Bernardo A. Nogueira

Received: 19 June 2023
Revised: 18 July 2023
Accepted: 20 July 2023
Published: 25 July 2023

1. Introduction

Nanoparticles often possess properties deviating from the bulk phase and, for that reason, also offer perspectives for novel applications [1,2]. The bulk form of magnesium oxide is primarily used for refractory cement [3] and flame retardants [4] due to its excellent temperature resistance, as well as food supplement [5], as a buffer for acids in mining industries [6], and occasionally as an electric insulator [7]. In contrast, MgO nanoparticles have paved the way for additional applications in the production of functional ceramics [8], the catalytic remediation of wastewater [9], carbon dioxide capture [10], gas sensors [11], antibacterial coatings [12], and their use in therapeutics [13] and drug delivery [14].

The high surface-to-volume ratio and the increase in sites with low coordination on the surface of nanoparticles, in particular on facets with high Miller indices, make them particularly efficient when it comes to catalytic activity [15,16]. Moreover, MgO nanoparticles, being chemically very stable, show excellent stability against catalyst poisoning: being highly reusable makes them eco-friendly.

And while the surface-related properties are often associated with the nominal surface of MgO, it has been reported for some time that these surfaces are also extremely sensitive to ambient humidity. The presence of water (as well as solid contaminants and various gases) can strongly affect the nominal MgO surface: what is considered a clean surface is not always so clean, in particular when the nanoparticles are stored under ambient conditions. MgO nanoparticles are particularly susceptible due to their extremely large surface-to-volume ratio.

MgO is a large band gap ionic oxide crystallizing in a face-centered cubic structure. Its surface chemistry has been extensively studied [17] as it is commonly used for heterogeneous catalysis and as a substrate for the growth of epitaxial films. MgO nanoparticles have recently attracted much attention [18]. The precise chemical control of its surface is thus a key point.

Syrlybekov et al. [19] have demonstrated that for a clean (001) single crystalline MgO bulk left for 8 months in ambient conditions, magnesium hydroxyl and carbonate are present on the surface. The preparation of a clean MgO surface is not simple, as this compound is hygroscopic [20]. Of course, in the case of nanoparticles, chemical transformations can occur much faster: Thomele et al. [21] have reported the formation of $Mg(OH)_2$ for MgO nanoparticles in the presence of water.

To get a better understating of the water-MgO interaction, numerical calculations have been performed [22–24]. Ončák et al. [25] have confirmed using DFT that a fully hydroxylated topmost MgO(001) is not stable and have proposed a surface reconstruction with Mg^{2+} ions above the surface. The pulling out from the surface of Mg atoms was proposed by Jug et al. [26] as a possible first step of $Mg(OH)_2$ layer formation on the MgO surface. It appears that the reactivity of MgO with water is high, and it should even be higher in the specific case of nanoparticles for which the surface-to-volume ratio is big. The question of the chemical mechanisms involved in the interaction between water and MgO remains open.

Raman spectroscopy is a powerful technique for the study of nanostructure surfaces [27]. For symmetry reasons, MgO has no first-order Raman mode [28]. Nevertheless, Ishikawa et al. [29] have reported four Raman modes for MgO microcrystals in the 200–1200 cm^{-1} spectral region. They proposed different hypotheses for the origin of these unattended modes: relaxation of selection rules and phonons at the zone boundary. They suggested that these modes result from the MgO itself and have not considered the possible chemical reactivity of nanoparticles with species present in the ambient air. In particular, they have not paid attention to the OH spectral region (around 3600 cm^{-1}), a key spectral region in the case of water adsorption.

In this article, we propose to focus on the Raman spectrum in the specific -OH region of MgO surfaces in interaction with water molecules. We performed DFT calculations for different water adsorption configurations and compared them with the experimental spectrum of MgO nanoparticles stored in ambient air. Our results clearly confirm the high reactivity of MgO with water. This feature should be taken into account for the interpretation of the Raman spectrum of MgO nanoparticles.

2. Methods

DFT calculations have been performed with Crystal Software [30,31]. Firstly, a two-dimensional slab of 4 layers of MgO crystal (space group 225, fcc structure and lattice parameter of 4.21 Å) has been cut at atomic planes (001), (011) and (112). For the low-density water coverage (1 adsorbed water molecule per 2 MgO unit cell on the top layer), three different configurations have been simulated: H_2O on MgO(001) slab, H_2O on MgO(011) slab and H_2O on MgO(112) slab. For high-density water coverage (2 adsorbed water molecules per unit cell of 17 $Å^2$), only one configuration consisting of H_2O over MgO(001) surface has been simulated. Those configurations offer a good compromise between efficiency and calculation cost. The final optimized atoms coordinates can be found in the supplementary information. We have used the hybrid B3LYP Hamiltonian [32,33] plus D3-dispersion [34], associated with a double-zeta plus polarization atomic orbital basis set adapted for periodic systems [35]. Basis sets were directly chosen from the Crystal library [36] for Mg [37], O [38,39] and H [40]. We have also reported the results obtained with the same basis set but adding a d-orbital on Mg (0.4 $bohr^{-2}$) and O (0.5 $bohr^{-2}$).

Firstly, a self-consistent field (SCF) calculation is performed in order to obtain the unperturbed energy and electron density after geometry optimization, and then the Coupled Perturbed Hartree—Fock and Kohn—Sham (CPHF/CPKS) method implemented in Crystal is used to determine the Raman intensities [41,42], followed by the harmonic calculation of the vibrational modes with their frequency [43,44]. Anharmonic correction of the Raman spectrum will also be conducted using the vibrational self-consistent field (VSCF) plus vibrational configurational interaction (VCI) models implemented in the CRYSTAL code [45–47].

For the Raman experiments, high-purity MgO nanoparticles (99+%) of nominal size of 20 nm (US Research Nanomaterials Inc.) have been used. Raman spectra were performed on a Horiba spectrometer (iHR320) system with a 473 nm laser, an objective of 50× and a grating of 2400 L/mm (1 cm^{-1} typical spectral resolution). The exposition time was 120 s, with 3 spectra acquired for averaging in order to obtain the best signal-to-noise ratio. The spectrometer was calibrated with the spectral lines of a xenon lamp.

3. Results and Discussion

The water molecule has three Raman active modes: one symmetric bending mode (A_1 symmetry), observed at around 1600 cm^{-1}, and two stretching modes (symmetric A_1 and antisymmetric B_2), giving rise to a broad experimental band between 3000 and 3600 cm^{-1}. MgO has no first-order Raman active modes.

In ambient air, water is easily adsorbed on the surface of MgO nanoparticles. Figure 1 shows the experimental Raman spectrum of MgO nanoparticles in the OH stretching region, and at least four modes are observed (3650, 3670, 3710 and 3730 cm^{-1}), confirming the presence of water on the MgO surface. Compared to the standard Raman spectrum of free water, those modes are shifted towards higher wavenumber due to the specific interaction between water and the MgO surface. Surprisingly they are also much thinner than what is observed with free water, typically 10 cm^{-1} for the 3650 cm^{-1} peak.

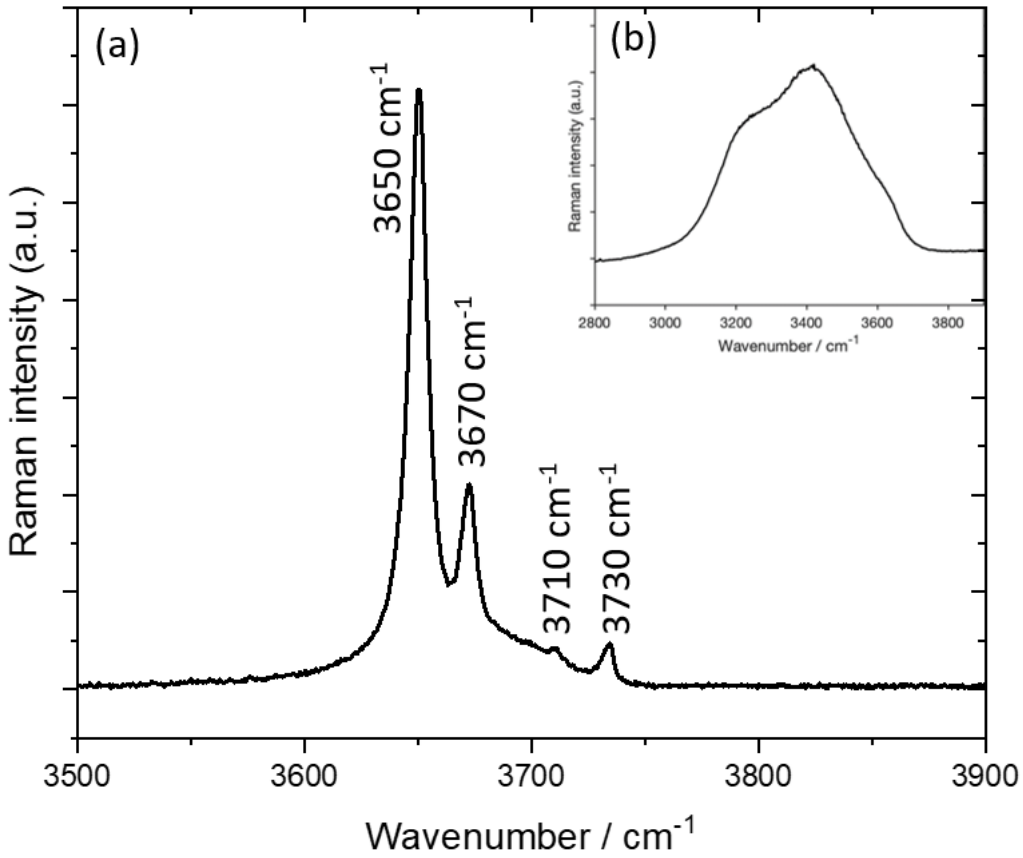

Figure 1. (**a**) Typical Raman spectrum of MgO nanoparticles in the OH stretching region. (**b**) Raman spectrum of liquid water in the same spectral range.

Those experimental measurements prove the interaction of water with the MgO surface. It also demonstrates that Raman spectroscopy is a powerful method for the study of nanoparticles' surface reactivity.

Nevertheless, the exact origin of those modes remains unclear. To push forward the analysis of Raman spectra of MgO nanoparticles in the OH region, we performed DFT

calculations of water molecules on MgO with different configurations. We have studied the effect of the crystallographic surface of MgO, the density of water molecules adsorption, and the possible chemical reactions between water and MgO. For each situation, we calculated the Raman spectra and compared them with what was experimentally reported.

MgO has three simple surfaces: (001), (011) and (111). Due to charge surfaces, the (111) surface is unstable and cannot be considered. We first performed DFT calculations of harmonic Raman modes of a water molecule adsorbed on a (001) MgO surface, a configuration that has already been reported in many publications [48–50]. The optimized geometry and the calculated spectrum are shown in Figure 2 for the smallest basis set (without d-orbital on O and Mg).

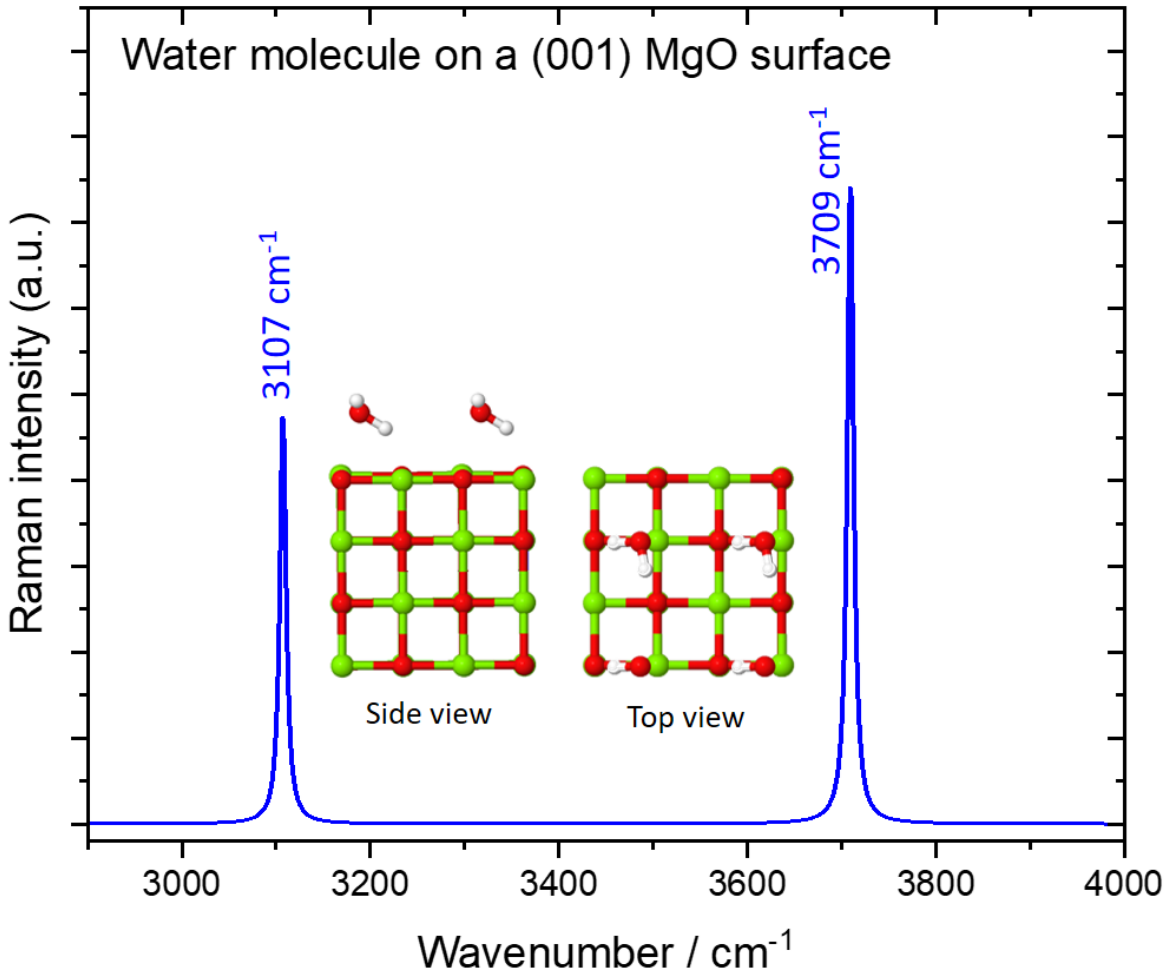

Figure 2. Calculated configuration and Raman spectra for a (001) MgO surface. Green balls corresponds to Mg atoms, red balls to O atoms and white balls to H atoms.

The oxygen atom is above an Mg atom, whereas one of the two hydrogen atoms tends to point towards surface oxygen with a hydrogen bond of ~1.8 Å. The water molecule does not lie flat on the surface but is slightly tilted. Those results are in good accordance with what was reported by Gardeh et al. [51] with the Vienna ab initio simulation package for DFT calculations and Alessio et al. [52] with a hybrid quantum mechanics approach. The top layer of Mg and O atoms is also slightly deformed by the presence of the water molecule. Jong Wan Lee [53] has also reported the top layer deformation of MgO surfaces in interaction with carbon and hydrogen using a first-principles quantum mechanical code. From our simulation, one can also notice that the H_2O molecule is not dissociated. The mode at 3709 cm^{-1} is the Raman O-H stretching mode of the hydrogen that is tilted away from the MgO surface, while the mode at 3107 cm^{-1} is the O-H stretching mode of the hydrogen

that is pointing towards the MgO surface. One can notice that the former frequency value is much higher than that of the hydrogen pointing towards the MgO surface, which is due to the fact that the hydrogen pointing away from the surface is more free than the one pointing towards the MgO surface. The hydrogen that is pointing toward the MgO surface probably forms a weak hydrogen bond with the oxygen of the MgO surface (see the view from the top on Figure 2). Therefore its stretching mode (3107 cm^{-1}) is lower. We can safely assume that there is physisorption of H_2O on the MgO(001) surface, and thus no chemical reaction with MgO(001). Anyway, the two reported modes at 3107 and 3709 cm^{-1} cannot explain the four modes shown in Figure 1.

Another possibility is to consider a higher coverage of water molecules on the MgO(001) surface. In the configuration shown in Figure 2, the density of water molecules (1 adsorbed molecule per unit cell of 17 $Å^2$) is too low for interaction between adsorbed molecules themselves. Thus, the final geometry of the system is purely governed by the molecule-surface interaction. Figure 3 shows the calculated configuration with a double density of water molecules on the MgO(001) surface.

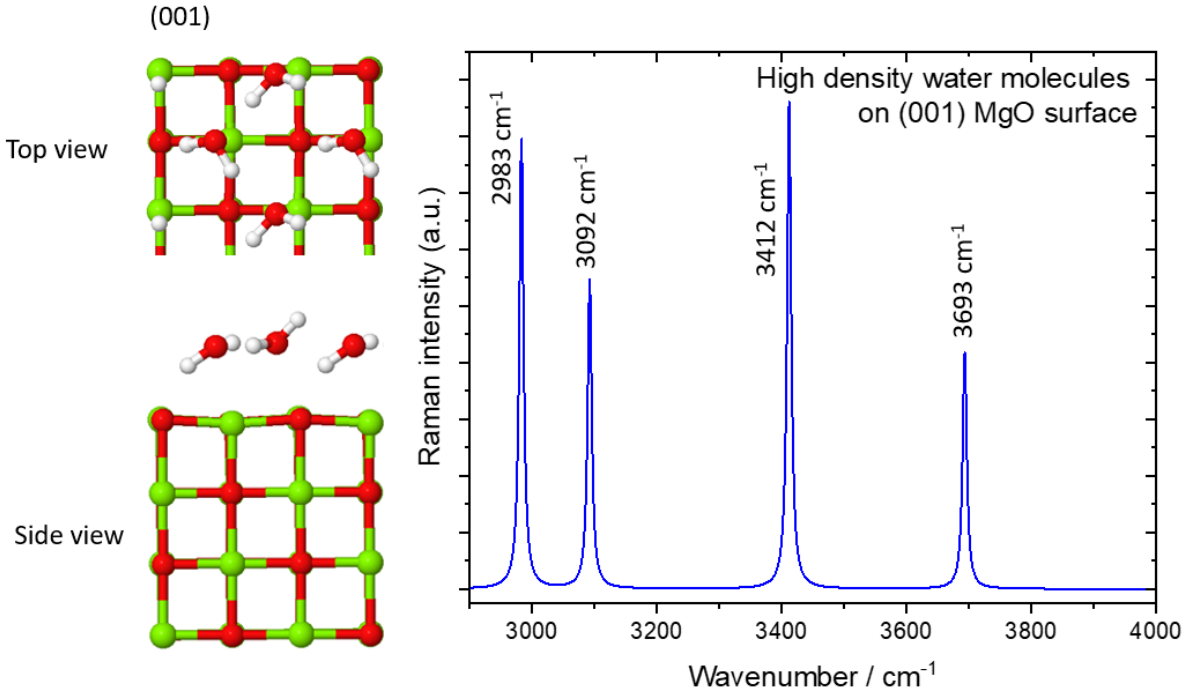

Figure 3. Calculated configuration and Raman spectra for a higher density of water molecules on a (001) MgO surface. Green balls corresponds to Mg atoms, red balls to O atoms and white balls to H atoms.

This time, due to higher intermolecular interactions, water molecules adopt different orientation angles towards the MgO surface. Therefore, the doublet of OH modes is split into four modes. Nevertheless, even if we observe four modes, their splitting is greater than what is experimentally measured. In addition, several peaks appear below 3500 cm^{-1}, not observed in experimental Raman spectra. This configuration leads to Raman spectra that are quite different from what is measured.

The last situation is the chemical reactivity of MgO with water. Due to their high surface-to-volume ratio, nanoparticles are much more reactive than bulk materials. Thus water molecules can react with MgO surfaces to form $Mg(OH)_2$. Jug et al. [26] have proposed a process for the $Mg(OH)_2$ formation based on a pulling-out mechanism of Mg atoms from the surface. In our previous calculations, we have not observed such a feature: the stability of the (001) surfaces is very high towards reactivity with water.

As mentioned above, we thus considered the more reactive (011) and (112) surfaces. After energy optimization, we observed dissociation of the water molecule with bridge Mg-

O(H)-Mg and (Mg)O-H covalent bonds, as can be seen in Figure 4. This result confirms the higher reactivity of (011) and (112) surfaces, in comparison with the (001), independently from any pulling-out mechanism. This dissociation can be considered as a first step towards the transformation of MgO into $Mg(OH)_2$ as both the OH and H resulting react with the MgO surface. The MgO surface itself is highly deformed.

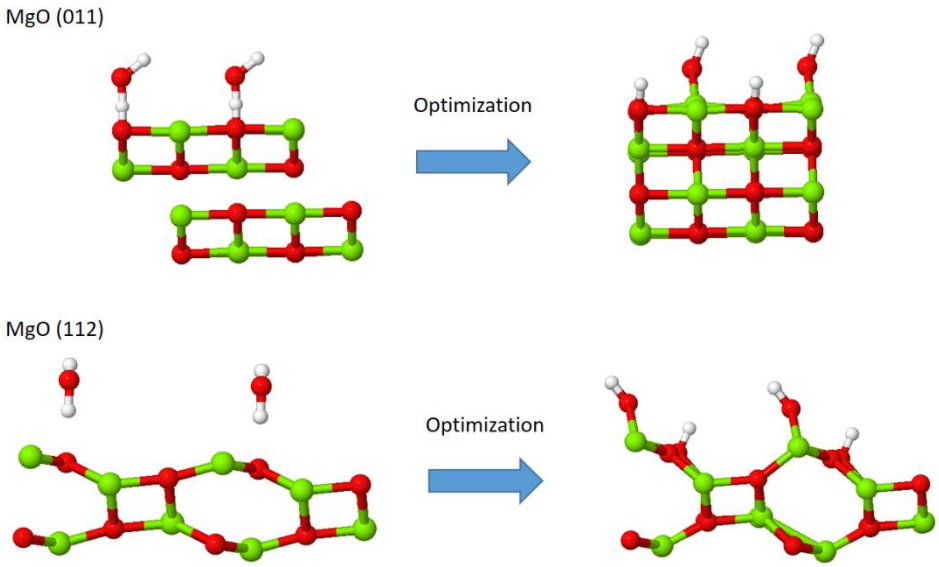

Figure 4. Energy optimization of the MgO(011) and (112) surfaces in interaction with water molecules. Green balls corresponds to Mg atoms, red balls to O atoms and white balls to H atoms.

We have then calculated the harmonic Raman spectrum of both surfaces, and the obtained spectra are shown in Figure 5 (small basis set, without d-orbitals on O and Mg).

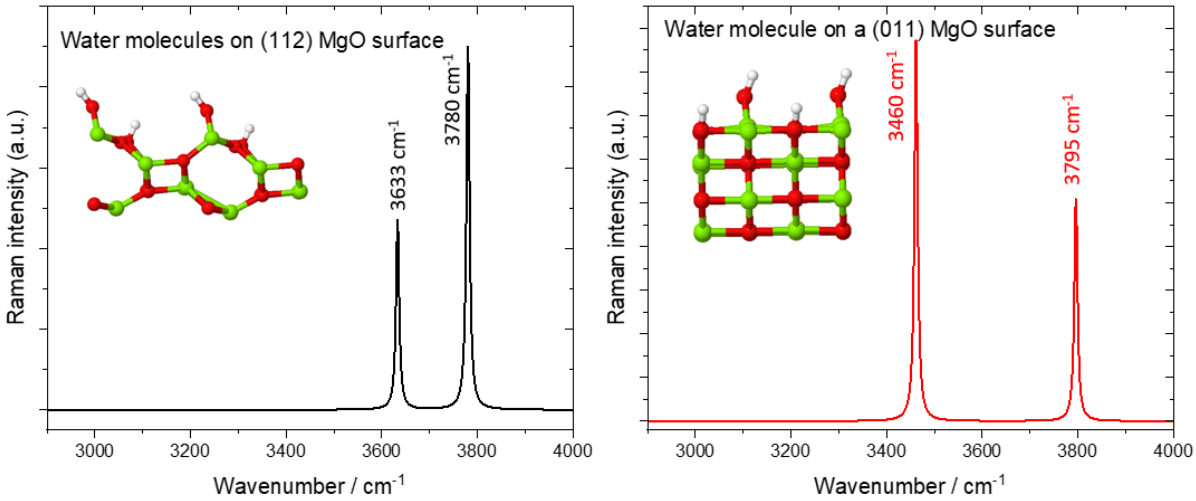

Figure 5. Calculated Raman spectrum of the MgO(112) and (011) surfaces in interaction with water molecules after energy optimization. Green balls corresponds to Mg atoms, red balls to O atoms and white balls to H atoms.

Two vibrational modes are present in the OH region, for both surfaces, with wavenumbers very close to what is experimentally observed (Figure 1). Those two modes are the stretching O-H modes of the dissociated water molecule. For the MgO(011) surface, the highest mode, 3795 cm^{-1}, corresponds to the O-H stretching mode of the OH that is attached to the Mg of the surface, while the 3460 cm^{-1} corresponds to the O-H stretching mode of the hydrogen that is bound to the oxygen of the MgO surface. One can observe

that the same goes for the MgO(112) surface: the highest mode, 3780 cm^{-1}, corresponds to the stretching mode of the hydroxyl that is attached to the MgO surface, and the lowest mode, 3633 cm^{-1}, is the stretching of the hydrogen that is bound to the surface oxygen.

To push forward our calculations, we have now considered the anharmonicity. Calculations of Raman modes for free H_2O are reported in Table 1 for both the smallest basis set and the basis set with d orbitals. It appears clearly that an anharmonic treatment of the modes is necessary to be conducted for a better agreement with the experiment. For the clarity of the discussion, we have also considered $Mg(OH)_2$ (brucite) in its P-3m1 space group (164).

Table 1. Wavenumber (in cm^{-1})/Raman intensities (in $Å^4$ amu^{-1}) of water, brucite and H_2O on MgO. Values in parentheses are obtained with the smallest basis set without d-orbitals on Mg and O.

Configuration	Frequencies/Intensities	
	Harmonic	**Anharmonic**
H_2O	3846/30, 3731/86 (3778/28, 3649/87)	3684/31, 3603/86 (3619/29, 3527/87)
1 H_2O/MgO(001)	3768/103, 3321/67	3672/108, 3182/67
2 H_2O/MgO(001)	3753/104, 3618/245 3378/242, 3126/122	3654/106, 3481/270 3182/228, 2947/138
H_2O-MgO(011)	3805/102, 3584/114	3701/106, 3397/112
H_2O-MgO(112)	3816/125, 3696/68	3724/130, 3603/70
$Mg(OH)_2$ (brucite)	3805/459 (3746/405)	3676/455 (3611/391)

Indeed, as reported in Figure 2 of Ref. [54] for water and in Table 2 of Ref. [55] for brucite, differences between harmonic and experimental frequency values can be larger than 150 cm^{-1}, showing the important anharmonic red-shift effect on frequencies.

The anharmonic results reported in Table 1 have been obtained from the VSCF/VCI method leading to the following frequency/intensity: 3684 cm^{-1}/31 $Å^4$ amu^{-1} and 3603 cm^{-1}/86 $Å^4$ amu^{-1} for the two highest frequency peaks of water with d-orbital on O (3619 cm^{-1}/29 $Å^4$ amu^{-1} and 3527 cm^{-1}/87 $Å^4$ amu^{-1} without d-orbital on O) and, 3676 cm^{-1}/455 $Å^4$ amu^{-1} for the highest frequency peak of the brucite Raman spectrum with d-orbitals on O and Mg (3611 cm^{-1}/391 $Å^4$ amu^{-1} without d-orbitals), in much better agreement with experimental results.

However, even if the anharmonic correction is important on the Raman frequencies of water and brucite, red-shifting the highest Raman frequency by around 130 cm^{-1} for brucite, the Raman intensities are less affected by it. For water adsorption on the (001) MgO surface, peaks below 3500 cm^{-1} remains present and cannot be retained in the interpretation of the experimental Raman spectrum (Figure 1). It appears that the Raman modes calculated with the more reactive (011) and (112) surfaces are much closer to the experimental ones, as can be seen in Figure 6.

Now that we have calculated the Raman spectra in the OH region for different interactions of water with MgO surfaces, we can make a hypothesis for the explanation of the experimental spectrum of MgO nanoparticles, as shown in Figure 1. $Mg(OH)_2$ (brucite) has a single Raman mode [56] around 3650 cm^{-1}, as reported in Figure 6. We can reasonably assume that a part of MgO has reacted with water from the ambient air and has been transformed into brucite, giving rise to the intense Raman mode at 3650 cm^{-1}. This chemical transformation has been reported by Leung et al. [57], and our study proves that it can be easily identified through Raman spectroscopy. This result confirms the high potentiality of Raman spectroscopy for the characterization of nanoparticles.

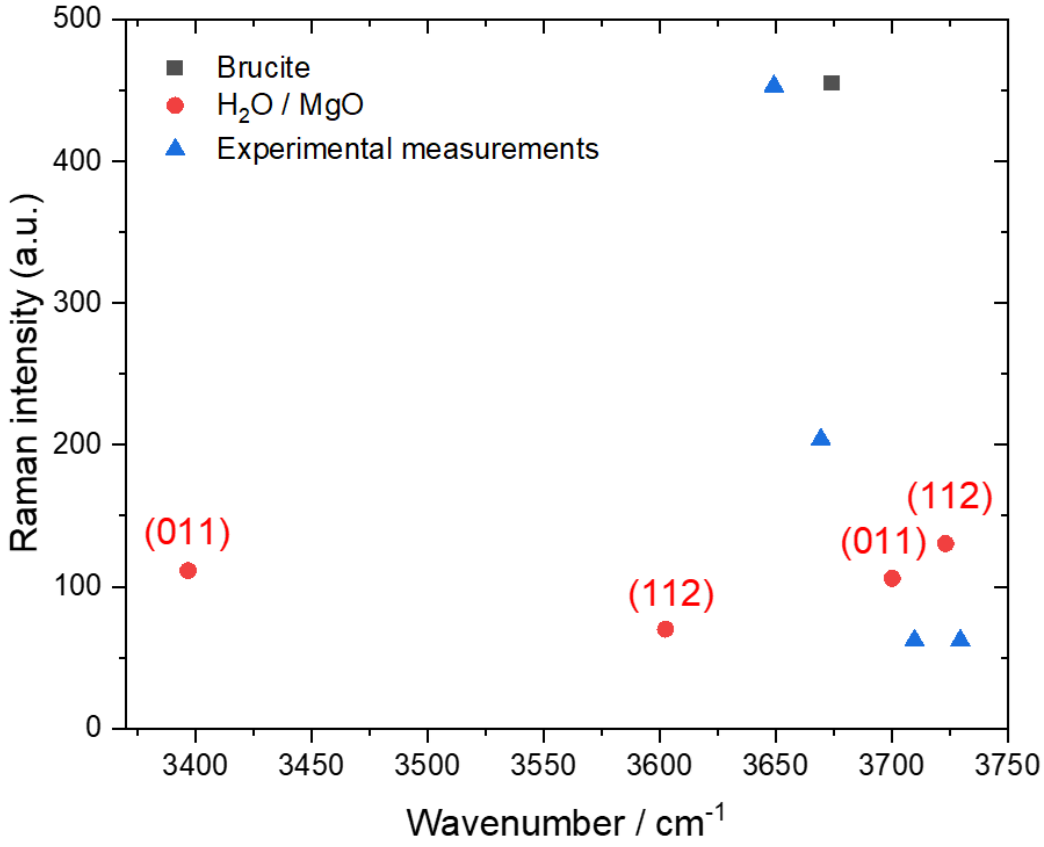

Figure 6. Final comparison of calculated Raman modes for brucite and water on MgO(011) and (112) surfaces. Anharmonicty and d-orbitals on Mg and O are taken into account. The experimental modes, as observed in Figure 1, are also reported.

However, this feature is not enough to explain the observed higher frequency modes. Based on our calculations on the (112) and (011) surfaces, we assume that those modes are associated with intermediate species formed during the adsorption and dissociation of water molecules. For the (011) surface, a mode is still present below 3500 cm^{-1}. This surface is stable, with rather low reactivity, and the Raman signature of its chemical reaction with water is not experimentally observed. However, for the (112) surface, in addition to the 3603 cm^{-1}, surely masked by the intense brucite mode in the experimental spectra, we also observed a mode at 3724 cm^{-1}, very close to the measured one at 3730 cm^{-1}. This mode can reasonably be attributed to the chemical species formed on this surface, as shown in Figure 4.

In conclusion, we propose to attribute all the modes higher than 3650 cm^{-1} to those chemical species resulting from the reaction between water and MgO surface. This suggests that the dissociation of water is the first step towards the transformation of MgO into $Mg(OH)_2$. The intermediate species formed are stable enough to be observed by Raman spectroscopy. Our study proves that:

- The reactivity of MgO nanoparticles with water present in the ambient air is very high. Brucite ($Mg(OH)_2$) is rapidly formed.
- The first step for the transformation of MgO into $Mg(OH)_2$ is the dissociation of water.
- Intermediate species resulting from this dissociation can be identified through Raman spectroscopy.

As MgO is extensively used for various applications (see the introduction part), its surface reactivity, demonstrated here with water, should be systematically considered. When it is stored in ambient air, MgO reacts rapidly with water to form various surface species. In the specific case of nanoparticles, for which the surface-to-volume ratio is very

high, those reactions lead to the formation of brucite. Of course, the chemical properties of the formed species are different from the standard MgO surface and will affect its efficiency, in particular for catalytic applications. To avoid this problem, we strongly recommend paying attention to the storage conditions of MgO, ideally in dry air, in particular in its nanoparticle form.

Supplementary Materials: The following supporting information can be downloaded at: https://www.mdpi.com/article/10.3390/cryst13081153/s1.

Author Contributions: Conceptualization, A.M. and A.R.; software, M.R. and M.D.; validation, A.M.; formal analysis, M.D., A.M. and M.D.; supervision, A.M and A.R. All authors have read and agreed to the published version of the manuscript.

Funding: We acknowledge the "Direction du Numérique" of the "Université de Pau et des Pays de l'Adour" and the Mésocentre de Calcul Intensif Aquitain (MCIA) for the computing facilities provided.

Data Availability Statement: Not applicable.

Conflicts of Interest: The authors declare no conflict of interest.

References

1. Xu, H.; Guan, D.; Ma, L. The bio-inspired heterogeneous single-cluster catalyst Ni100–Fe_4S_4 for enhanced electrochemical CO_2 reduction to CH_4. *Nanoscale* **2023**, *15*, 2756–2766. [CrossRef]
2. Lv, Z.; Xu, H.; Xu, W.; Peng, B.; Zhao, C.; Xie, M.; Lv, X.; Gao, Y.; Hu, K.; Fang, Y.; et al. Quasi-Topological Intercalation Mechanism of $Bi_{0.67}NbS_2$ Enabling 100 C Fast-Charging for Sodium-Ion Batteries. *Adv. Energy Mater.* **2023**, *13*, 2300790. [CrossRef]
3. Obregón, Á.; Rodríguez-galicia, J.L.; López-cuevas, J.; Pena, P.; Baudín, C. MgO—$CaZrO_3$-based refractories for cement kilns. *J. Eur. Ceram. Soc.* **2011**, *31*, 61–74. [CrossRef]
4. Li, X.; Zhang, K.; Shi, R.; Ma, X.; Tan, L.; Ji, Q.; Xia, Y. Enhanced flame-retardant properties of cellulose fibers by incorporation of acid-resistant magnesium-oxide microcapsules. *Carbohydr. Polym.* **2017**, *176*, 246–256. [CrossRef]
5. Carpenter, T.O.; Delucia, M.C.; Zhang, J.H.; Bejnerowicz, G.; Tartamella, L.; Dziura, J.; Petersen, K.F.; Befroy, D.; Cohen, D. A Randomized Controlled Study of Effects of Dietary Magnesium Oxide Supplementation on Bone Mineral Content in Healthy Girls. *J. Clin. Endocrinol. Metab.* **2006**, *91*, 4866–4872. [CrossRef] [PubMed]
6. Kastyuchik, A.; Karam, A.; Aïder, M. Environmental Technology & Innovation Effectiveness of alkaline amendments in acid mine drainage remediation. *Environ. Technol. Innov.* **2016**, *6*, 49–59. [CrossRef]
7. Kathrein, H.; Freund, F.J. Electrical conductivity of magnesium oxide single crystal below 1200 K. *Phys. Chem. Solids* **1983**, *44*, 177–186. [CrossRef]
8. Itatani, K.; Tsujimoto, T.; Kishimoto, A. Thermal and optical properties of transparent magnesium oxide ceramics fabricated by post hot-isostatic pressing. *J. Eur. Ceram. Soc.* **2006**, *26*, 639–645. [CrossRef]
9. Fouda, A.; Hassan, S.E.; Abdel-rahman, M.A.; Farag, M.M.S.; Shehal-deen, A.; Mohamed, A.A.; Alsharif, S.M.; Saied, E.; Moghanim, S.A.; Salah, M. Current Research in Biotechnology Catalytic degradation of wastewater from the textile and tannery industries by green synthesized hematite (α-Fe_2O_3) and magnesium oxide (MgO) nanoparticles. *Curr. Res. Biotechnol.* **2021**, *3*, 29–41. [CrossRef]
10. Song, G.; Zhu, X.; Chen, R.; Liao, Q.; Ding, Y.; Chen, L. An investigation of CO_2 adsorption kinetics on porous magnesium oxide. *Chem. Eng. J.* **2016**, *283*, 175–183. [CrossRef]
11. Hornak, J. Synthesis, Properties, and Selected Technical Applications of Magnesium Oxide Nanoparticles: A Review. *Int. J. Mol. Sci.* **2021**, *22*, 12752. [CrossRef]
12. Naguib, G.H.; Nassar, H.M.; Hamed, M.T. Bioactive Materials Antimicrobial properties of dental cements modified with zein-coated magnesium oxide nanoparticles. *Bioact. Mater.* **2022**, *8*, 49–56. [CrossRef]
13. Fernandes, M.; RB Singh, K.; Sarkar, T.; Singh, P.; Pratap Singh, R. Recent Applications of Magnesium Oxide (MgO) Nanoparticles in various domains. *Adv. Mater. Lett.* **2020**, *11*, 1–10. [CrossRef]
14. Sastry, S.V.; Nyshadham, J.R.; Fix, J.A. Recent technological advances in oral drug delivery—A review. *PSTT* **2000**, *3*, 138–145. [CrossRef] [PubMed]
15. Xu, H.; Guan, D. Exceptional Anisotropic Noncovalent Interactions in Ultrathin Nanorods: The Terminal σ-Hole. *ACS Appl. Mater. Interfaces* **2022**, *14*, 51190–51199. [CrossRef] [PubMed]
16. Xu, H.; Liu, P.; Zhang, W.; Wang, Q.; Yang, Y. Structure, stability, electronic and magnetic properties of monometallic Pd, Pt, and bimetallic Pd-Pt core—Shell nanoparticles. *Chem. Phys.* **2020**, *539*, 110953. [CrossRef]
17. Khairallah, F.; Glisenti, A. Synthesis, characterization and reactivity study of nanoscale magnesium oxide. *J. Mol. Catal. A Chem.* **2007**, *274*, 137–147. [CrossRef]

18. Singh, J.P.; Singh, V.; Sharma, A.; Pandey, G.; Chae, K.H.; Lee, S. Approaches to synthesize MgO nanostructures for diverse applications. *Heliyon* **2020**, *6*, e04882. [CrossRef]
19. Syrlybekov, A.; Arca, E.; Verre, R.; O Coileain, C.; Toktarbaiuly, O.; Khalid, A.; Zhang, H.; Shvets, I.V. Induced morphological changes on vicinal MgO (100) subjected to high-temperature annealing: Step formation and surface stability. *Surf. Interface Anal.* **2015**, *47*, 969–977. [CrossRef]
20. Geler-Kremer, J.; Posadas, A.B.; Demkov, A.A. Preparation of clean MgO surface by oxygen plasma: Comparison with standard substrate cleaning procedures. *J. Vac. Sci. Technol. B* **2020**, *38*, 062201. [CrossRef]
21. Thomele, D.; Gheisi, A.R.; Niedermaier, M.; Elsässer, M.S.; Bernardi, J.; Grönbeck, H.; Diwald, O. Thin water films and particle morphology evolution in nanocrystalline MgO. *J. Am. Ceram. Soc.* **2018**, *101*, 4994–5003. [CrossRef] [PubMed]
22. Ding, Z.; Selloni, A. Hydration structure of flat and stepped MgO surfaces. *J. Chem. Phys.* **2021**, *154*, 114708. [CrossRef] [PubMed]
23. Kebede, G.G.; Spångberg, D.; Mitev, P.D.; Broqvist, P.; Hermansson, K. Comparing van der Waals DFT methods for water on NaCl (001) and MgO (001). *J. Chem. Phys.* **2017**, *146*, 064703. [CrossRef]
24. Chen, J.; Huang, L.; Dong, L.; Zhang, H.; Huang, Z.; Li, F.; Zhang, S. Hydration behavior of MgO surface: A first-principles study. *Appl. Surf. Sci.* **2023**, *611*, 155441. [CrossRef]
25. Ončák, M.; Włodarczyk, R.; Sauer, J. Water on the MgO (001) surface: Surface reconstruction and ion solvation. *J. Phys. Chem. Lett.* **2015**, *6*, 2310–2314. [CrossRef]
26. Jug, K.; Heidberg, B.; Bredow, T. Molecular Dynamics Study of Water Adsorption Structures on the MgO (100) Surface. *J. Phys. Chem. C* **2007**, *111*, 6846–6851. [CrossRef]
27. Hadj Youssef, A.; Zhang, J.; Ehteshami, A.; Kolhatkar, G.; Dab, C.; Berthomieu, D.; Merlen, A.; Légaré, F.; Ruediger, A. Symmetry-Forbidden-Mode Detection in $SrTiO_3$ Nanoislands with Tip-Enhanced Raman Spectroscopy. *J. Phys. Chem. C* **2021**, *125*, 6200–6208. [CrossRef]
28. Manson, N.B.; Von der Ohe, W.; Chodos, S.L. Second-Order Raman Spectrum of MgO. *Phys. Rev. B* **1971**, *3*, 1968. [CrossRef]
29. Ishikawa, K.; Fujima, N.; Komura, H. First-order Raman scattering in MgO microcrystals. *J. Appl. Phys.* **1985**, *57*, 973–975. [CrossRef]
30. Dovesi, R.; Erba, A.; Orlando, R.; Zicovich-Wilson, C.M.; Civalleri, B.; Maschio, L.; Rérat, M.; Casassa, S.; Baima, J.; Salustro, S.; et al. Quantum-mechanical condensed matter simulations with CRYSTAL. *Wiley Interdiscip. Rev. Comput. Mol. Sci.* **2018**, *8*, e1360. [CrossRef]
31. Dovesi, R.; Pascale, F.; Civalleri, B.; Doll, K.; Harrison, N.M.; Bush, I.; D'Arco, P.; Noel, Y.; Rera, M.; Carbonniere, P.; et al. The CRYSTAL code, 1976–2020 and beyond, a long story. *J. Chem. Phys.* **2020**, *152*, 204111. [CrossRef] [PubMed]
32. Becke, A.D. Density-functional thermochemistry. III. The role of exact exchange. *J. Chem. Phys.* **1993**, *98*, 5648. [CrossRef]
33. Lee, C.; Yang, W.; Parr, R.G. Development of the collesalvetti correlation-energy formula into a functional of the electron density. *Phys. Rev. B* **1988**, *37*, 785. [CrossRef]
34. Grimme, S.; Antony, J.; Ehrlich, S.; Krieg, H. A consistent and accurate ab initio parametrization of density functional dispersion correction (DFT-D) for the 94 elements H-Pu. *J. Chem. Phys.* **2010**, *132*, 154104. [CrossRef]
35. Vilela Oliveira, D.; Laun, J.; Peintinger, M.F.; Bredow, T. BSSE-correction scheme for consistent gaussian basis sets of double- and triple-zeta valence with polarization quality for solid-state calculations. *J. Comput. Chem.* **2019**, *40*, 2364–2376. [CrossRef]
36. Available online: https://www.crystal.unito.it/basis_sets.html (accessed on 24 July 2023).
37. McCarthy, M.I.; Harrison, N.M. Ab Initio determination of the bulk properties of MgO. *Phys. Rev. B* **1994**, *49*, 8574–8582. [CrossRef]
38. Scaranto, J.; Giorgianni, S. A quantum-mechanical study of CO adsorbed on TiO_2: A comparison of the Lewis acidity of the rutile (1 1 0) and the anatase (1 0 1) surfaces. *J. Mol. Struct.* **2008**, *858*, 72–76. [CrossRef]
39. Towler, M.D.; Allan, N.L.; Harrison, N.M.; Saunders, V.R.; Mackrodt, W.C.; Apra, E. An ab initio Hartree-Fock study of MnO and NiO. *Phys. Rev. B* **1994**, *50*, 5041–5054. [CrossRef] [PubMed]
40. Dovesi, R.; Ermondi, E.; Ferrero, E.; And, C.P.; Roetti, C. Hartree-Fock study of lithium hydride with the use of a polarizable basis set. *Phys. Rev. B* **1983**, *29*, 3591–3600. [CrossRef]
41. Maschio, L.; Kirtman, B.; Rérat, M.; Orlando, R.; Dovesi, R. Ab initio analytical Raman intensities for periodic systems through a coupled perturbed Hartree-Fock/Kohn-Sham method in an atomic orbital basis. I. Theory. *J. Chem. Phys.* **2013**, *139*, 164101. [CrossRef]
42. Maschio, L.; Kirtman, B.; Rérat, M.; Orlando, R.; Dovesi, R. Ab initio analytical Raman intensities for periodic systems through a coupled perturbed Hartree-Fock/Kohn-Sham method in an atomic orbital basis. II. Validation and comparison with experiments. *J. Chem. Phys.* **2013**, *139*, 164102. [CrossRef]
43. Pascale, F.; Zicovich-Wilson, C.M.; López Gejo, F.; Civalleri, B.; Orlando, R.; Dovesi, R. The calculation of the vibrational frequencies of crystalline compounds and its implementation in the CRYSTAL code. *J. Comput. Chem.* **2004**, *25*, 888–897. [CrossRef]
44. Zicovich-Wilson, C.M.; Pascale, F.; Roetti, C.; Saunders, V.R.; Orlando, R.; Dovesi, R. Calculation of the vibration frequencies of α-quartz: The effect of hamiltonian and basis set. *J. Comput. Chem.* **2004**, *25*, 1873–1881. [CrossRef] [PubMed]
45. Erba, A.; Maul, J.; Ferrabone, M.; Carbonniere, P.; Rerat, M.; Dovesi, R. Anharmonic Vibrational States of Solids from DFT Calculations. Part I: Description of the Potential Energy Surface. *J. Chem. Theory Comput.* **2019**, *15*, 3755–3765. [CrossRef] [PubMed]

46. Erba, A.; Maul, J.; Ferrabone, M.; Dovesi, R.; Rerat, M.; Carbonniere, P. Anharmonic Vibrational States of Solids from DFT Calculations. Part II: Implementation of the VSCF and VCI Methods. *J. Chem. Theory Comput.* **2019**, *15*, 3766–3777. [CrossRef] [PubMed]
47. Carbonniere, P.; Erba, A.; Richter, F.; Dovesi, R.; Rérat, M. Calculation of Anharmonic IR and Raman Intensities for Periodic Systems from DFT Calculations: Implementation and Validation. *J. Chem. Theory Comput.* **2020**, *16*, 3343–3351. [CrossRef] [PubMed]
48. Heidberg, J.; Redlich, B.; Wetter, D. Adsorption of Water Vapor on the MgO (100) Single Crystal Surface. *Phys. Chem.* **1995**, *11*, 1333–1337. [CrossRef]
49. Odelius, M. Mixed Molecular and Dissociative Water Adsorption on MgO [100]. *Phys. Rev. Lett.* **1999**, *82*, 3919–3922. [CrossRef]
50. Xu, C.; Goodman, D.W. Structure and geometry of water adsorbed on the MgO (100) surface. *Chem. Phys. Lett.* **1997**, *265*, 341–346. [CrossRef]
51. Gardeh, M.G.; Kistanov, A.A.; Nguyen, H.; Manzano, H.; Cao, W.; Kinnunen, P. Exploring Mechanisms of Hydration and Carbonation of MgO and $Mg(OH)_2$ in Reactive Magnesium Oxide-Based Cements. *J. Phys. Chem. C* **2022**, *126*, 6196–6206. [CrossRef] [PubMed]
52. Alessio, M.; Usvyat, D.; Sauer, J. Chemically Accurate Adsorption Energies: CO and H_2O on the MgO (001) Surface. *J. Chem. Theory Comput.* **2019**, *15*, 1329–1344. [CrossRef] [PubMed]
53. Lee, J.W. Effect of C and H contamination on the MgO surface properties studied using the first-principles method. *J. Inf. Disp.* **2013**, *14*, 97–102. [CrossRef]
54. Broda, M.A.; Buczek, A.; Kupka, T.; Kaminsky, J. Anharmonic vibrational frequency calculations for solvated molecules in the B3LYP Kohn—Sham basis set limit. *Vib. Spectrosc.* **2012**, *63*, 432–439. [CrossRef]
55. Pascale, F.; Tosoni, S.; Zicovich-wilson, C.; Ugliengo, P.; Orlando, R.; Dovesi, R. Vibrational spectrum of brucite, $Mg(OH)_2$: A periodic ab initio quantum mechanical calculation including OH anharmonicity. *Chem. Phys. Lett.* **2004**, *396*, 308–315. [CrossRef]
56. Available online: https://rruff.info/Brucite/R050455 (accessed on 24 July 2023).
57. Leung, Y.H.; Ng, A.M.C.; Xu, X.; Shen, Z.; Gethings, L.A.; Wong, M.T.; Chan, C.M.N.; Guo, M.Y.; Ng, Y.H.; Djurisic, A.B.; et al. Mechanisms of Antibacterial Activity of MgO Non-ROS Mediated Toxicity of MgO Nanoparticles Towards *Escherichia coli*. *Small* **2014**, *10*, 1171–1183. [CrossRef]